# Chapter 6

# TRIBO-CORROSION BEHAVIOUR

*This chapter presents the outcomes of tribo-corrosion testing, focusing on techniques such as Open Circuit Potential (OCP) and Potentiodynamic Polarization (PDP). It provides a detailed analysis of the tribo-corrosion behavior of different alloy systems, highlighting variations in their electrochemical performance under sliding conditions. These findings are crucial for assessing the suitability of the alloys for applications requiring enhanced durability and corrosion resistance, such as biomedical implants and structural components.*

## 6.1 Tribocorrosion behaviour of cpTi and Ti-6Al-4V

The tribocorrosion results for OCP test are shown in Fig. 6.1(a) and for PDP shown in Fig. 6.1(b). It indicates that Ti-6Al-4V exhibits superior tribocorrosion resistance compared to cpTi due to its alloying elements (Al and V), which enhance the stability and self-healing of its passive oxide layer. In the OCP profile (Fig. 6.1(a)), Ti-6Al-4V shows a higher and more stable potential, suggesting better corrosion resistance and less disruption of the oxide layer during wear. The coefficient of friction for Ti-6Al-4V is also lower, indicating smoother sliding and less mechanical damage compared to cpTi. In the potentiodynamic polarization curve (Fig. 6.1(b)), Ti-6Al-4V has a lower current density and a more extended passive region, signifying reduced anodic dissolution and enhanced electrochemical stability. In contrast, cpTi shows greater potential fluctuations, higher current densities, and higher friction coefficients, reflecting its higher susceptibility to both mechanical wear and electrochemical degradation. indicate that cpTi and Ti-6Al-4V exhibit different wear characteristics under OCP and PDP conditions. The wear track profile obtained after tribocorrosion test for cpTi and Ti-6Al-4V are shown in Fig. 6.2 and corresponding values of wear

track width, wear track area, and wear volume are given in Table 6.1. For both materials, wear volume and cross-sectional area of the wear scar are higher under PDP conditions compared to OCP, which suggests an accelerated material removal due to the combined effects of mechanical wear and electrochemical degradation. The higher wear volume and scar width for cpTi under PDP (0.491 $mm^3$, 1814.82 µm) compared to Ti-6Al-4V (0.341 $mm^3$, 1606.03 µm) indicate that cpTi is more susceptible to tribocorrosion in corrosive environments. This can be attributed to the absence of alloying elements like Al and V in cpTi, which provide enhanced mechanical strength and corrosion resistance to Ti-6Al-4V. Additionally, the larger wear scar width and volume in PDP conditions are indicative of increased anodic dissolution caused by the applied potential, weakening the material's resistance to wear.

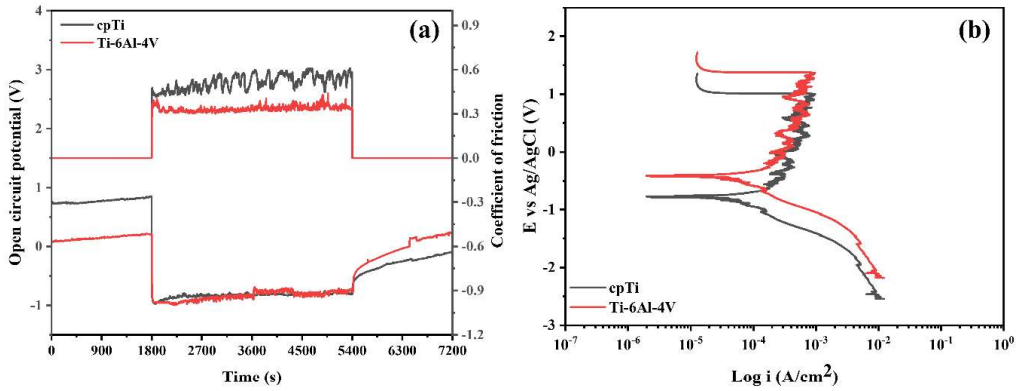


**Fig. 6.1:** Tribocorrosion response of cpTi and Ti-6Al-4V (a) OCP test, (b) PDP test

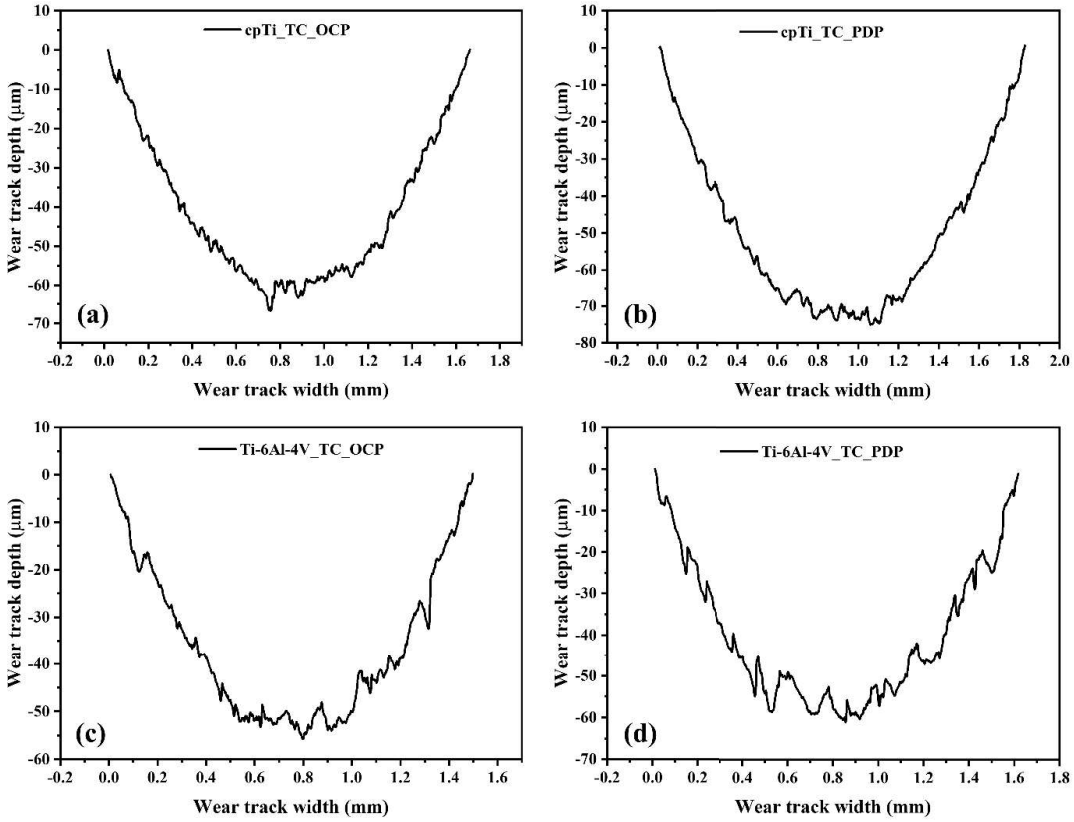


**Fig. 6.2:** Wear track profile after tribocorrosion test of cpTi and Ti-6Al-4V for OCP and PDP test

**Table 6.1:** Wear parameters resulting from tribo-corrosion test in OCP and PDP test for cpTi and Ti-6Al-4V

| Samples | Wear scar cross-sectional area $A_w$ (μm$^2$) | Width of wear scar W (μm) | Wear volume (mm$^3$) |
|---|---|---|---|
| cpTi_OCP | 67594.45 | 1646.82 | 0.364 |
| cpTi_PDP | 90553.54 | 1814.82 | 0.491 |
| Ti-6Al-4V_OCP | 53842.05 | 1489.95 | 0.289 |
| Ti-6Al-4V_PDP | 63357.41 | 1606.03 | 0.341 |

### 6.2 Tribocorrosion behaviour of sintered binary alloys

The tribocorrosion results for Ti-Nb alloys are shown in Fig. 6.3 and corresponding wear profile is shown in Fig. 6.5. The influence of Nb content on the electrochemical and tribological performance of these alloys may be observed. From the Fig. 6.3(a) it is observed that alloys with lower Nb content exhibit higher and more stable potentials, indicating enhanced passivation and superior resistance to corrosion. This improvement can be attributed to Nb's ability to stabilize the β-phase and enhance the formation of a protective oxide layer. Conversely, alloys with higher Nb content, such as Ti-20Nb and Ti-25Nb, show lower potentials and greater fluctuations, signifying less effective passivation and higher susceptibility to wear-induced damage. The potentiodynamic polarization curves shown in Fig. 6.3(b) reveals that the current density decreases with increasing Nb content, suggesting increased material dissolution rates and lower electrochemical stability.

Additionally, the coefficients of friction for lower Nb-containing alloys are lower, indicating smoother sliding behavior and reduced wear. These results highlighted that increasing Nb content improves the tribocorrosion resistance of Ti-10Nb alloys, making them suitable for biomedical applications where both mechanical wear and electrochemical stability are critical. The wear parameters for Ti-Nb alloys demonstrates that the wear performance is significantly influenced by the Nb content. Ti-10Nb shows the lowest wear volume (0.111 $mm^3$) and cross-sectional area of the wear scar (21285.57 $\mu m^2$), indicating superior wear resistance. This can be attributed to an optimal balance of mechanical properties and a stable oxide layer formation due to its Nb content. On the other hand, alloys with higher Nb content, such as Ti-20Nb and Ti-25Nb, exhibit increased wear volumes (0.271 $mm^3$ and 0.186 $mm^3$, respectively) and larger cross-sectional areas, likely due to reduced hardness as higher Nb contents

stabilize the β-phase, which is softer than the α-phase. Ti-15Nb also exhibits high wear volume (0.248 $mm^3$), possibly due to its intermediate Nb content, which might not provide sufficient hardness or oxide layer stability.

The results obtained from the OCP and PDP tribocorrosion test of Ti-Zr alloys are shown in Fig. 6.4 and corresponding wear profiles in Fig. 6.6. The wear parameters obtained from the tribo-corrosion tests under OCP and PDP conditions for Ti-xZr alloys reveal significant differences in wear behavior influenced by Zr content and test conditions. In the OCP test (Table 6.4), Ti-15Zr exhibited the lowest wear scar width (630.013 μm), cross-sectional area (2436.46 $\mu m^2$), and wear volume (0.0124 $mm^3$), indicating superior wear resistance compared to other compositions. In contrast, Ti-25Zr showed the highest wear parameters, likely due to increased material degradation at higher Zr content. Under PDP conditions given in Table 6.5, a similar trend was observed, with Ti-15Zr again displaying the best wear resistance, while Ti-25Zr recorded the highest wear scar width (942.966 μm), cross-sectional area (9508.9 $\mu m^2$), and wear volume (0.0491 $mm^3$).

The results suggest that moderate Zr content (e.g., Ti-15Zr) optimizes wear resistance, whereas excessive Zr content can lead to increased wear, potentially due to changes in microstructure and electrochemical instability. The PDP test generally resulted in lower wear parameters for most samples compared to OCP, likely due to the more protective behavior of the passive film formed under polarization conditions.

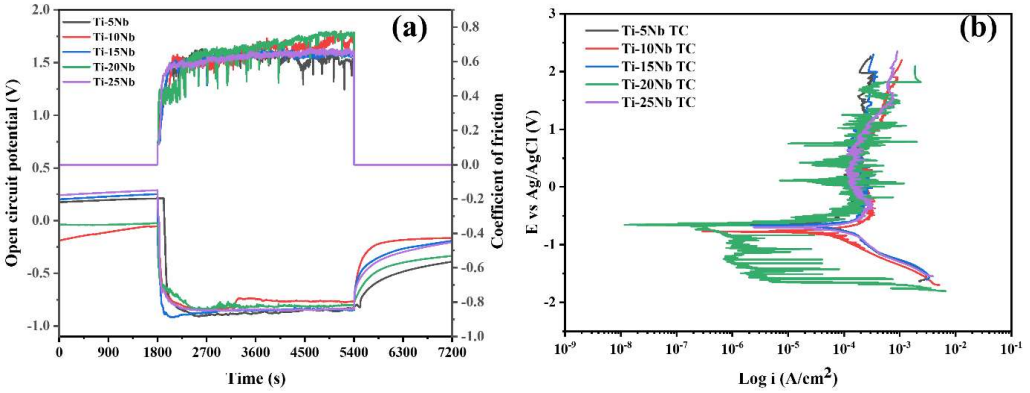


**Fig. 6.3:** Tribocorrosion response of binary Ti-xNb alloys (a) OCP test, (b) PDP test

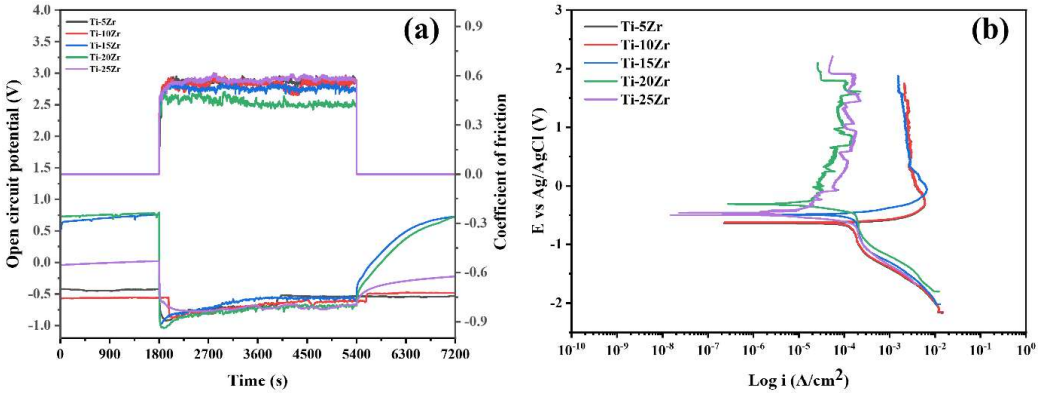


**Fig. 6.4:** Tribocorrosion response of binary Ti-xZr alloys (a) OCP test, (b) PDP test

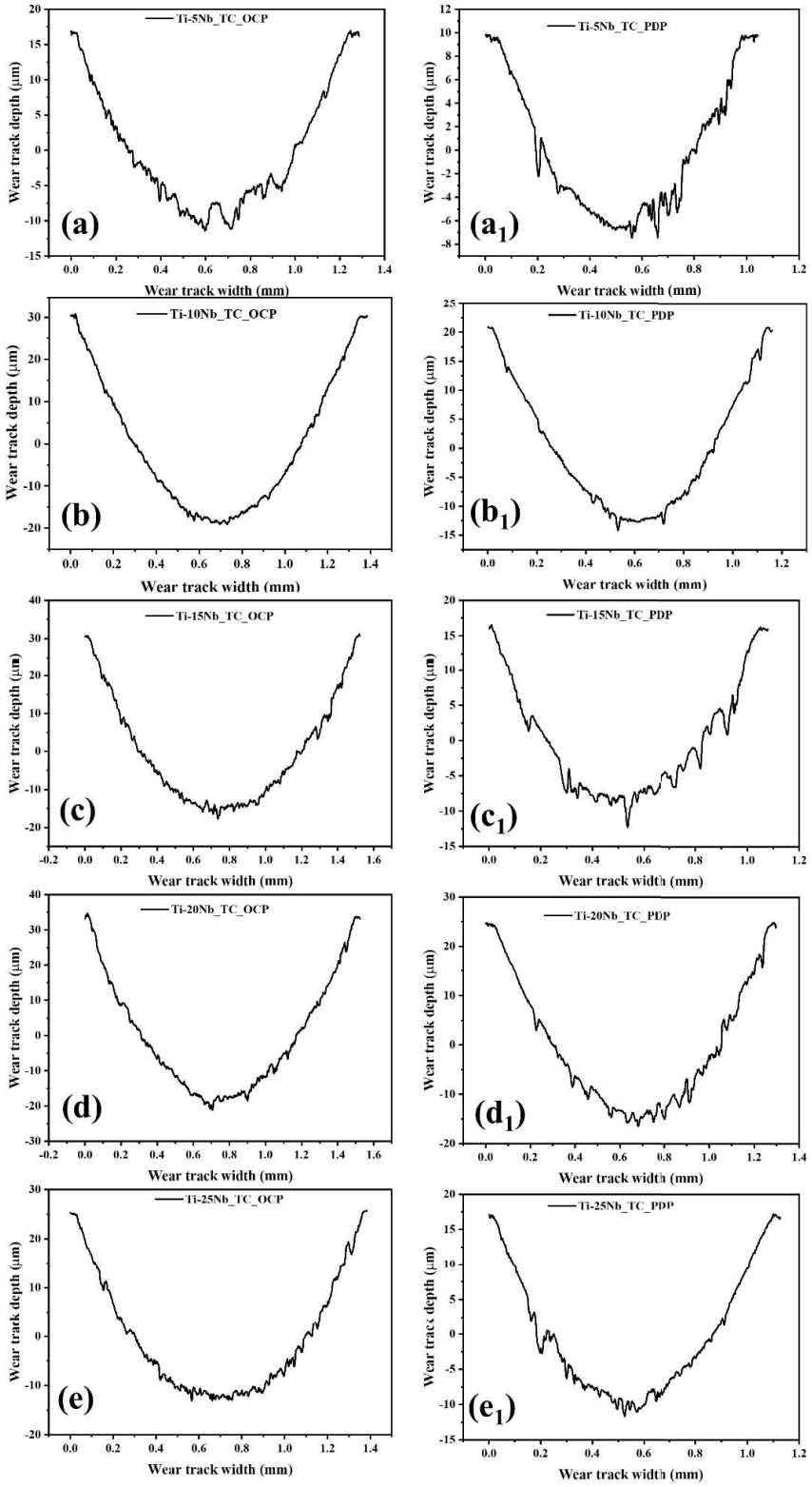


**Fig. 6.5:** Wear track profile after tribocorrosion test of Ti-xNb alloys for OCP and PDP test

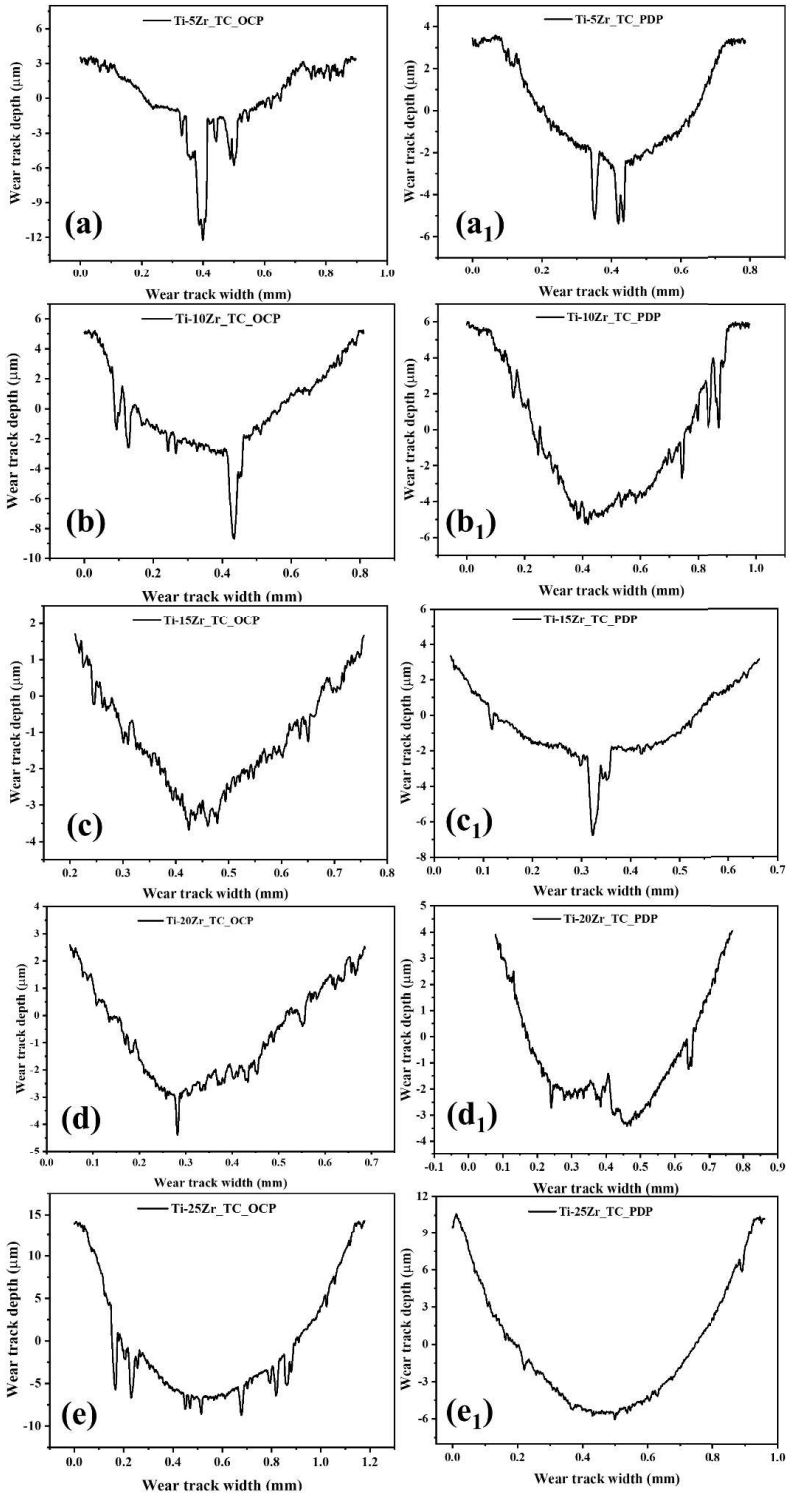


**Fig. 6.6:** Wear track profile after tribocorrosion test of Ti-xZr alloys for OCP and PDP test

**Table 6.2:** Wear parameters resulting from tribocorrosion test in OCP test of Ti-xNb alloys

| Samples | wear scar width W (µm) | Wear scar cross-sectional area $A_w$ (µm$^2$) | Wear volume (mm$^3$) |
|---|---|---|---|
| Ti-5Nb | 1332.29 | 42046.21 | 0.225 |
| Ti-10Nb | 1223.35 | 21285.57 | 0.1111 |
| Ti-15Nb | 1501.11 | 46608.69 | 0.2481 |
| Ti-20Nb | 1486.04 | 50578.59 | 0.2710 |
| Ti-25Nb | 1346.02 | 35222.58 | 0.1868 |

**Table 6.3:** Wear parameters resulting from tribocorrosion test in PDP test of Ti-xNb alloys

| Samples | wear scar width W (µm) | Wear scar cross-sectional area $A_w$ (µm$^2$) | Wear volume (mm$^3$) |
|---|---|---|---|
| Ti-5Nb | 1125.39 | 23927.68 | 0.1267 |
| Ti-10Nb | 936.05 | 10157.86 | 0.0526 |
| Ti-15Nb | 1042.08 | 17232.77 | 0.0904 |
| Ti-20Nb | 1245.54 | 31580.44 | 0.1679 |
| Ti-25Nb | 1092.79 | 18956.22 | 0.0995 |

**Table 6.4:** Wear parameters resulting from tribocorrosion test in OCP test of Ti-xZr alloys

| Samples | wear scar width W (µm) | Wear scar cross-sectional area $A_w$ (µm$^2$) | Wear volume (mm$^3$) |
|---|---|---|---|
| Ti-5Zr | 834.354 | 3115.31 | 0.0157 |
| Ti-10Zr | 922.909 | 5738.44 | 0.0292 |
| Ti-15Zr | 630.013 | 2436.46 | 0.0124 |
| Ti-20Zr | 690.008 | 3233.86 | 0.0165 |
| Ti-25Zr | 1170.458 | 16643.7 | 0.0863 |

**Table 6.5:** Wear parameters resulting from tribocorrosion test in PDP test of Ti-xZr alloys

| Samples | wear scar width W (µm) | Wear scar cross-sectional area $A_w$ (µm$^2$) | Wear volume (mm$^3$) |
|---|---|---|---|
| Ti-5Zr | 680.398 | 2629.64 | 0.0133 |
| Ti-10Zr | 795.077 | 4100.31 | 0.0209 |
| Ti-15Zr | 546.514 | 1574.66 | 0.0080 |
| Ti-20Zr | 635.008 | 2031.75 | 0.0103 |
| Ti-25Zr | 942.966 | 9508.9 | 0.0491 |

### 6.3 Tribocorrosion behaviour of sintered ternary alloys

The OCP and PDP response under tribocorrosion of ternary Ti-10Zr-xNb are shown in Fig. 6.7(a) and 6.7(b), and their wear profiles are shown in Fig. 6.8, respectively. The OCP results shows that the lower Nb content have higher potential, indicating better corrosion resistance. While higher Nb content reduce the potential, indicating lower corrosion resistance. The PDP response shows that the Ti-10Zr-10Nb has lower

corrosion current density under sliding wear. The wear parameters from tribocorrosion tests for Ti-10Zr-xNb alloys under OCP is given in Table 6.6 and for PDP Table 6.7 conditions demonstrate the influence of Nb content and test conditions on wear resistance. Under OCP, Ti-10Zr-10Nb showed the highest wear parameters, including wear scar width (2151.74 µm), cross-sectional area (265918.06 µm²), and wear volume (1.567 mm³), indicating poor wear resistance.

In contrast, Ti-10Zr-5Nb and Ti-10Zr-15Nb exhibited lower wear volumes of 0.1866 mm³ and 0.193 mm³, respectively, suggesting better wear performance. Under PDP conditions, wear resistance improved for all alloys, with Ti-10Zr-20Nb showing the lowest wear parameters (scar width: 1043.18 µm, cross-sectional area: 13247.15 µm², wear volume: 0.068 mm³), indicating superior protection likely due to enhanced passive film formation. The comparison highlights that increasing Nb content can either improve or degrade wear resistance depending on the alloy's microstructure and test conditions, with PDP tests generally yielding better wear performance due to enhanced electrochemical stability. Among all Ti-10Zr-xNb, Ti-10Zr-15Nb wear is lowest (optimum), which is mainly attributed to its softer Ti-Nb debris that comes in between the two mating surfaces and works as a lubricating agent between them by sacrificial exfoliation and resulting lower wear volume of this alloy.

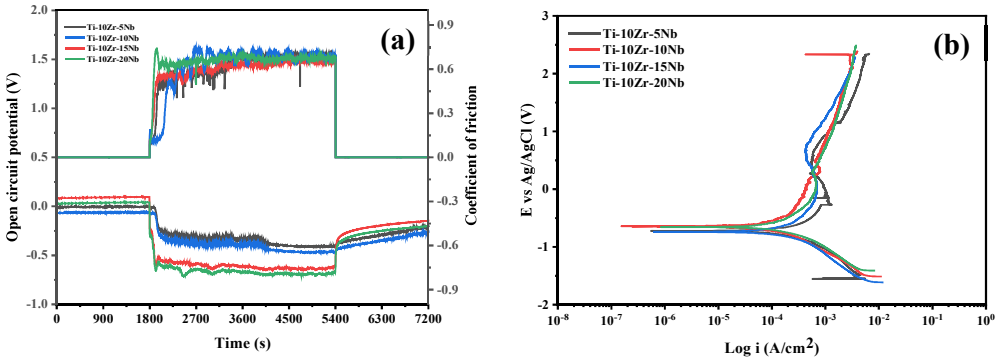


**Fig. 6.7:** Tribocorrosion response of ternary Ti-10Zr-xNb alloys (a) OCP test, (b) PDP

test

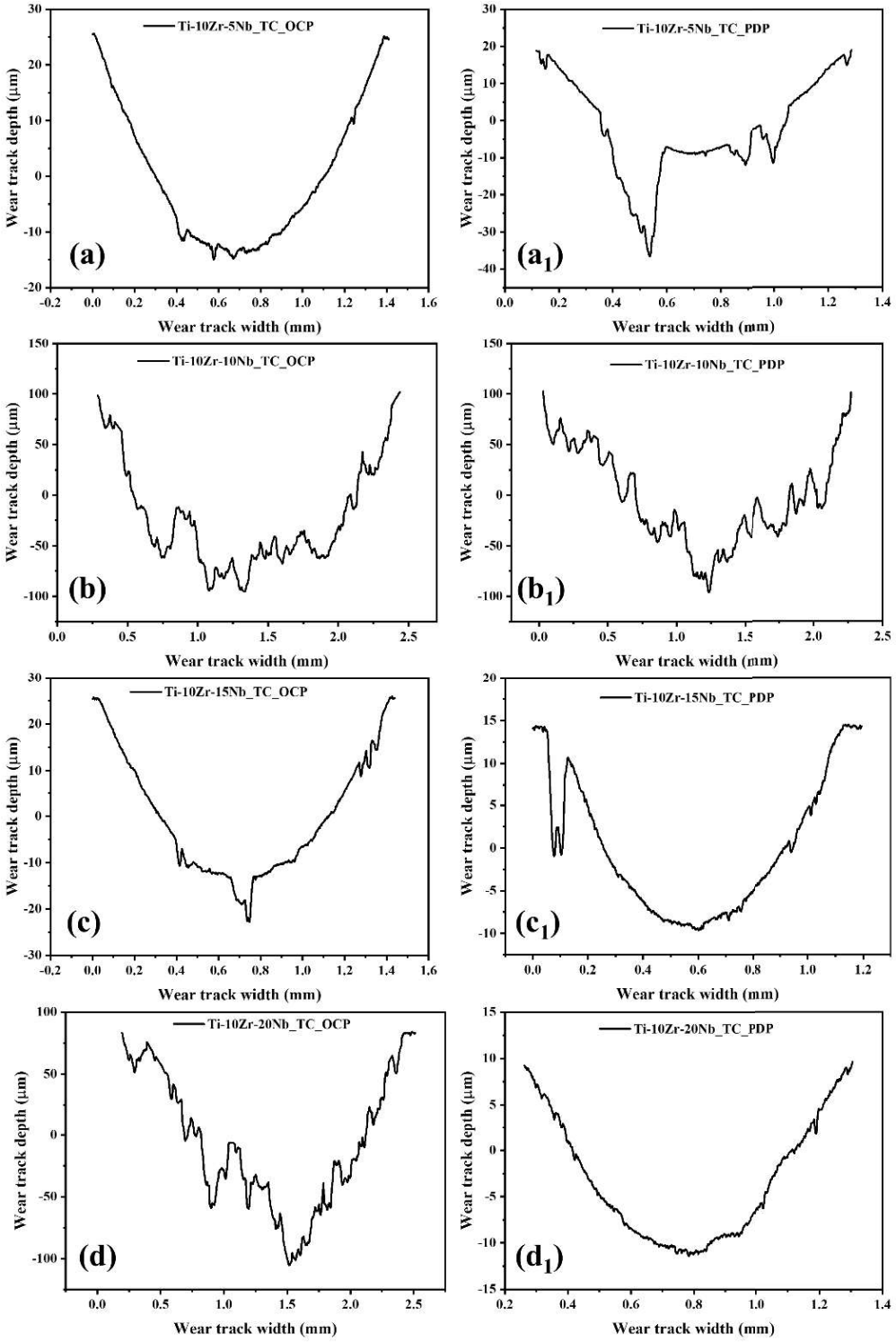


**Fig. 6.8:** Wear track profile after tribocorrosion test of Ti-10Zr-xNb alloys for OCP and PDP test

**Table 6.6:** Wear parameters resulting from tribocorrosion test in OCP test of Ti-10Zr-xNb alloys

| Samples | wear scar width W (µm) | Wear scar cross-sectional area $A_w$ (µm$^2$) | Wear volume (mm$^3$) |
|---|---|---|---|
| Ti-10Zr-5Nb | 1387.636 | 35292.01 | 0.1866 |
| Ti-10Zr-10Nb | 2151.74 | 265918.06 | 1.567 |
| Ti-10Zr-15Nb | 1419.5 | 36667.74 | 0.193 |
| Ti-10Zr-20Nb | 2295.242 | 207886.26 | 1.167 |

**Table 6.7:** Wear parameters resulting from tribocorrosion test in PDP test of Ti-10Zr-xNb alloys

| Samples | wear scar width W (µm) | Wear scar cross-sectional area $A_w$ (µm$^2$) | Wear volume (mm$^3$) |
|---|---|---|---|
| Ti-10Zr-5Nb | 1168.74 | 24614.28 | 0.130 |
| Ti-10Zr-10Nb | 2242.69 | 237210.21 | 1.360 |
| Ti-10Zr-15Nb | 1087.44 | 16977.73 | 0.088 |
| Ti-10Zr-20Nb | 1043.18 | 13247.15 | 0.068 |

### 6.4 Tribocorrosion behaviour of sintered high entropy alloys

The OCP response displayed in Fig. 6.9(a) of high entropy alloy shows a drastic breakdown of passive layer once the wear test is started and again shows passive layer formation after stopping the wear test. In contrast, wear and friction are significantly influenced by corrosion, suggesting a synergistic interaction between wear and corrosion. The wear profiles of HEAs are shown in Fig. 6.10 and their wear parameters from tribo-corrosion tests of under OCP and PDP conditions are shown in Tables 6.8 and 6.9, reveal the influence of different alloy compositions and test conditions on wear

performance. For HEA Cu, under OCP conditions, the wear scar was

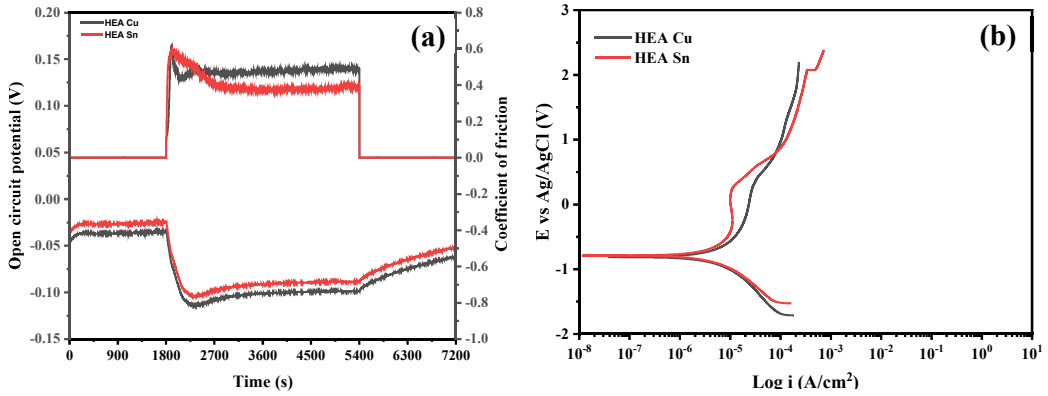


**Fig. 6.9:** Tribocorrosion response of HEAs (a) OCP test, (b) PDP test

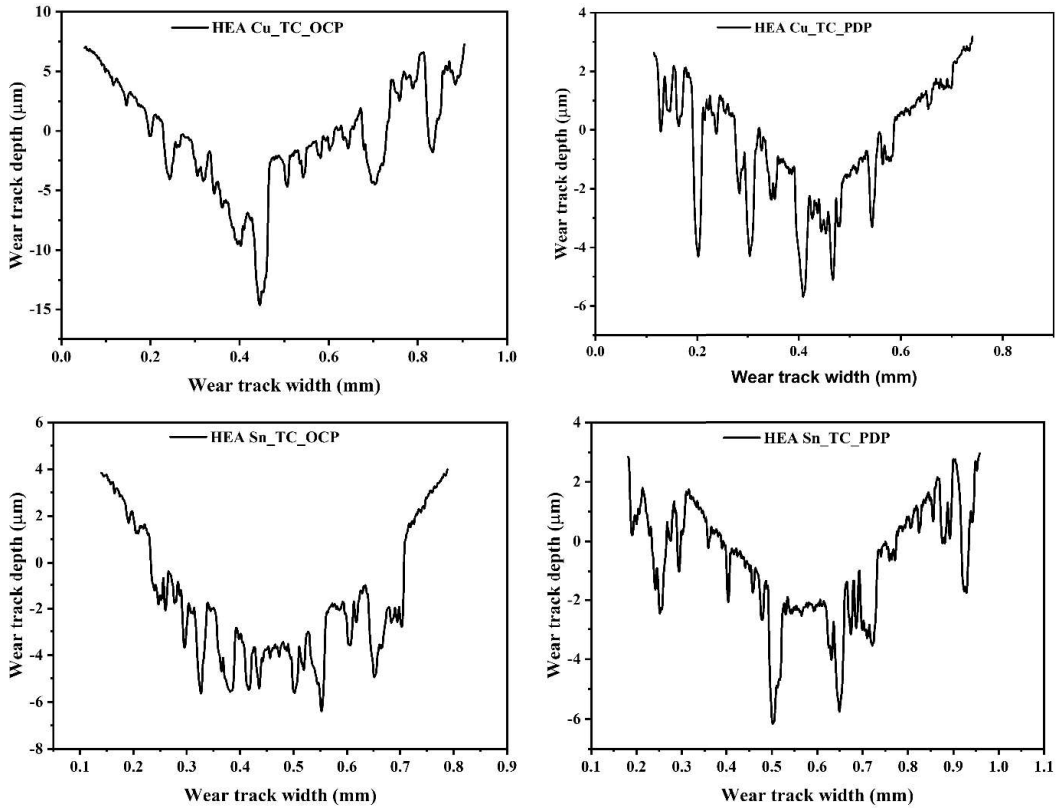


**Fig. 6.10:** Wear track profile after tribocorrosion test of high entropy alloys for OCP and PDP test of HEAs

**Table 6.8:** Wear parameters resulting from tribocorrosion test in OCP and PDP test of HEA Cu

| Samples | Wear scar cross-sectional area $A_w$ (µm²) | Width of wear scar W (µm) | Wear volume (mm³) |
|---|---|---|---|
| HEA Cu_OCP | 6564.93 | 849.511 | 0.0337 |
| HEA Cu_PDP | 2146.72 | 625.985 | 0.0109 |

**Table 6.9:** Wear parameters resulting from tribocorrosion test in OCP and PDP test of HEA Sn

| Samples | Wear scar cross-sectional area $A_w$ (µm²) | Width of wear scar W (µm) | Wear volume (mm³) |
|---|---|---|---|
| HEA Sn_OCP | 3604.09 | 649.003 | 0.0185 |
| HEA Sn_PDP | 2817.91 | 777.563 | 0.0142 |

significantly larger, with a cross-sectional area of 6564.93 µm², a width of 849.511 µm, and a wear volume of 0.0337 mm³, indicating higher wear compared to the PDP condition, where the wear scar dimensions were smaller (cross-sectional area: 2146.72 µm², width: 625.985 µm, wear volume: 0.0109 mm³). This reduction in wear under PDP is likely due to the formation of a more protective passive film during polarization, which decreases material degradation. Similarly, for HEA Sn, under OCP conditions, the wear scar cross-sectional area (3604.09 µm²), width (649.003 µm), and wear volume (0.0185 mm³) were higher than those observed in the PDP test, where the wear parameters were reduced (cross-sectional area: 2817.91 µm², width: 777.563 µm, wear volume: 0.0142 mm³). The comparison across both alloys indicates that PDP conditions generally lead to better wear resistance due to enhanced electrochemical stability,

resulting in smaller wear scars and lower wear volumes, as the passive film effectively reduces the interaction between the alloy surface and the counter material.

**6.5 Worn surface analysis of worn surfaces after tribocorrosion**

The tribocorrosion behaviour of cpTi and Ti-6Al-4V, as illustrated in Fig. 6.11, is governed by the synergistic interaction between mechanical wear and electrochemical corrosion. Under OCP, the protective passive oxide film is periodically disrupted by sliding contact, leading to localized depassivation followed by spontaneous repassivation. In contrast, under PDP, the externally applied anodic potential promotes continuous dissolution of the passive layer and inhibits effective repassivation, thereby exacerbating material degradation. For cpTi, the passive $TiO_2$ film is inherently less stable under anodic conditions, resulting in a more pronounced tribocorrosion effect. Ti-6Al-4V demonstrates relatively improved resistance owing to the stabilizing influence of alloying elements such as Al and V, which contribute to the formation of a more robust passive film. Nevertheless, both materials exhibit increased surface damage under PDP conditions, indicating that electrochemical activation significantly intensifies the material loss beyond that caused by mechanical wear alone.

The SEM images shown in Fig. 6.12 reveal that tribocorrosion mechanisms in Ti-xNb alloys vary significantly with Nb content and test conditions. Under OCP, Ti-10Nb shows the smoothest surface with shallow grooves, indicating mild oxidative wear and stable passive film formation. Ti-25Nb also exhibits moderate surface protection, while Ti-5Nb, Ti-15Nb, and Ti-20Nb display rougher surfaces with grooves, delamination, and debris, signs of dominant abrasive and adhesive wear due to unstable passivation. Under PDP, electrochemical polarization enhances passivation, with Ti-10Nb again showing the least surface damage, followed by Ti-25Nb and Ti-15Nb. In contrast, Ti-5Nb and Ti-20Nb show signs of passive film breakdown and increased wear. Overall,

the mechanism shifts from abrasive/adhesive wear in less stable alloys to oxidative wear in compositions with effective passivation, with Ti-10Nb demonstrating the most favourable tribocorrosion response.

The SEM images presented in Fig. 6.13 depict the worn surface morphology of Ti–xZr (x = 5, 10, 15, 20, 25 wt.%) alloys after tribocorrosion under OCP (a-e) and PDP ($a_1$–$e_1$) conditions. Under OCP conditions, the worn surfaces Fig. 6.13(a-e) exhibit more severe wear features such as delamination, surface grooves, pits, and accumulated debris, suggesting that passive films formed in freely corroding environments are mechanically unstable and prone to breakdown. These signs are more prominent in intermediate compositions like Ti-15Zr and Ti-20Zr, where partial oxide formation fails to sufficiently protect the surface. In contrast, the corresponding surfaces tested under PDP conditions Fig. 6.13($a_1$–$e_1$) show smoother topographies with fewer defects and less oxide debris, indicating that the electrochemical polarization promotes the formation of a stable and adherent oxide layer. This passive film acts as a barrier against mechanical and corrosive attack, thereby altering the tribocorrosion mechanism from aggressive abrasion to passivation-assisted wear resistance. The trend suggests that Zr addition improves corrosion protection during polarization, with Ti-25Zr (Fig. 6.13$e_1$) showing the most refined and protected surface.

The SEM micrographs shown in Fig. 6.14 illustrate the tribocorrosion mechanisms in Ti-10Zr-xNb alloys under OCP (a–d) and PDP ($a_1$–$d_1$) conditions. Under OCP, the worn surfaces (Fig. 6.14a–d) display prominent surface damage including oxide delamination, deep grooves, and debris accumulation, indicating that mechanical wear processes such as abrasion and adhesion dominate due to the unstable passive film. Particularly, Ti-10Zr-10Nb and Ti-10Zr-20Nb (Figs. 6.12b, d) exhibit more severe degradation, suggesting frequent passive film breakdown and active localized

corrosion. In contrast, the surfaces after PDP testing (Fig. 6.14$a_1$–$d_1$) appear markedly smoother with fewer wear features, confirming the formation of a more stable and protective oxide layer under anodic polarization. This promotes a transition in the tribocorrosion mechanism from mechanically driven degradation to repassivation-assisted wear mitigation, especially evident in Ti-10Zr-15Nb and Ti-10Zr-20Nb alloys (Figs. 6.12$c_1$, $d_1$).

The SEM analysis of the worn surfaces under tribocorrosion conditions shown in Fig. 6.15 revealed distinct degradation mechanisms for the two high-entropy alloys. Under OCP conditions, the $TiNb_{1.5}Mo_{1.1}Zr_{1.15}Cu_{0.25}$ alloy exhibited severe surface damage characterized by abrasive wear and debris accumulation, indicating dominant mechanical degradation due to limited passivation. In contrast, $TiNbZr_{0.8}Mo_{0.92}Sn_{0.28}$ showed relatively smoother surfaces with minimal wear, suggesting enhanced corrosion resistance, likely due to the presence of Sn. Under PDP conditions, both alloys demonstrated improved surface integrity, with $TiNb_{1.5}Mo_{1.1}Zr_{1.15}Cu_{0.25}$ forming a more protective oxide layer that mitigated wear, while $TiNbZr_{0.8}Mo_{0.92}Sn_{0.28}$ displayed minor localized pitting. These observations indicate that electrochemical polarization enhances tribocorrosion resistance by promoting repassivation, with $TiNbZr_{0.8}Mo_{0.92}Sn_{0.28}$ exhibiting superior stability under combined mechanical and electrochemical loading.

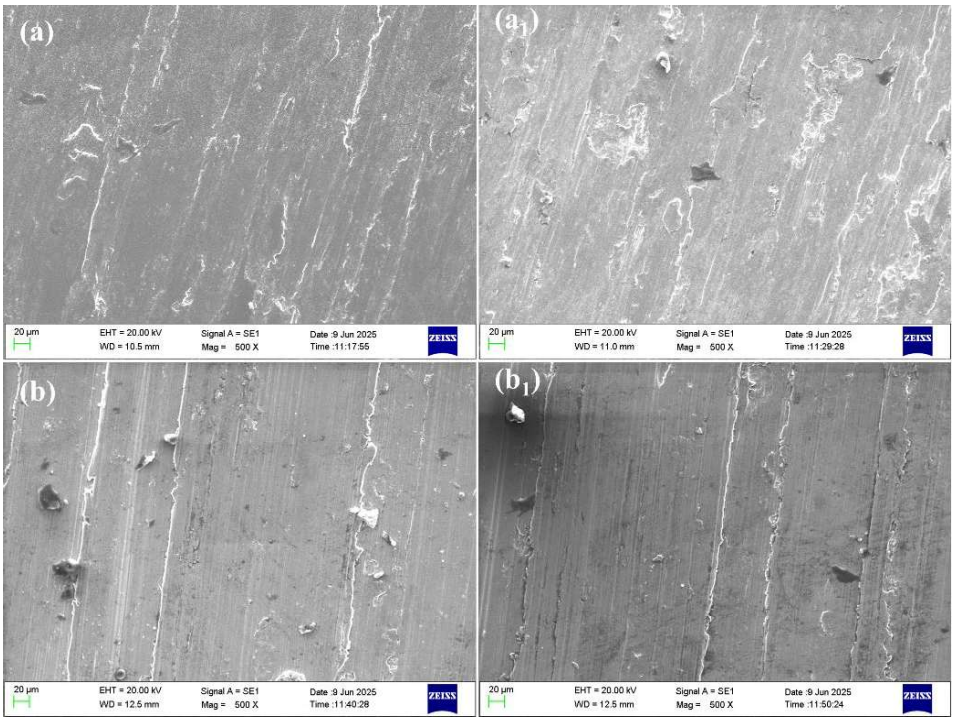


**Fig. 6.11:** Worn surfaces of (a) cpTi, (b) Ti-6Al-4V after OCP, and corresponding ($a_1$-$b_1$) for PDP tribocorrosion test

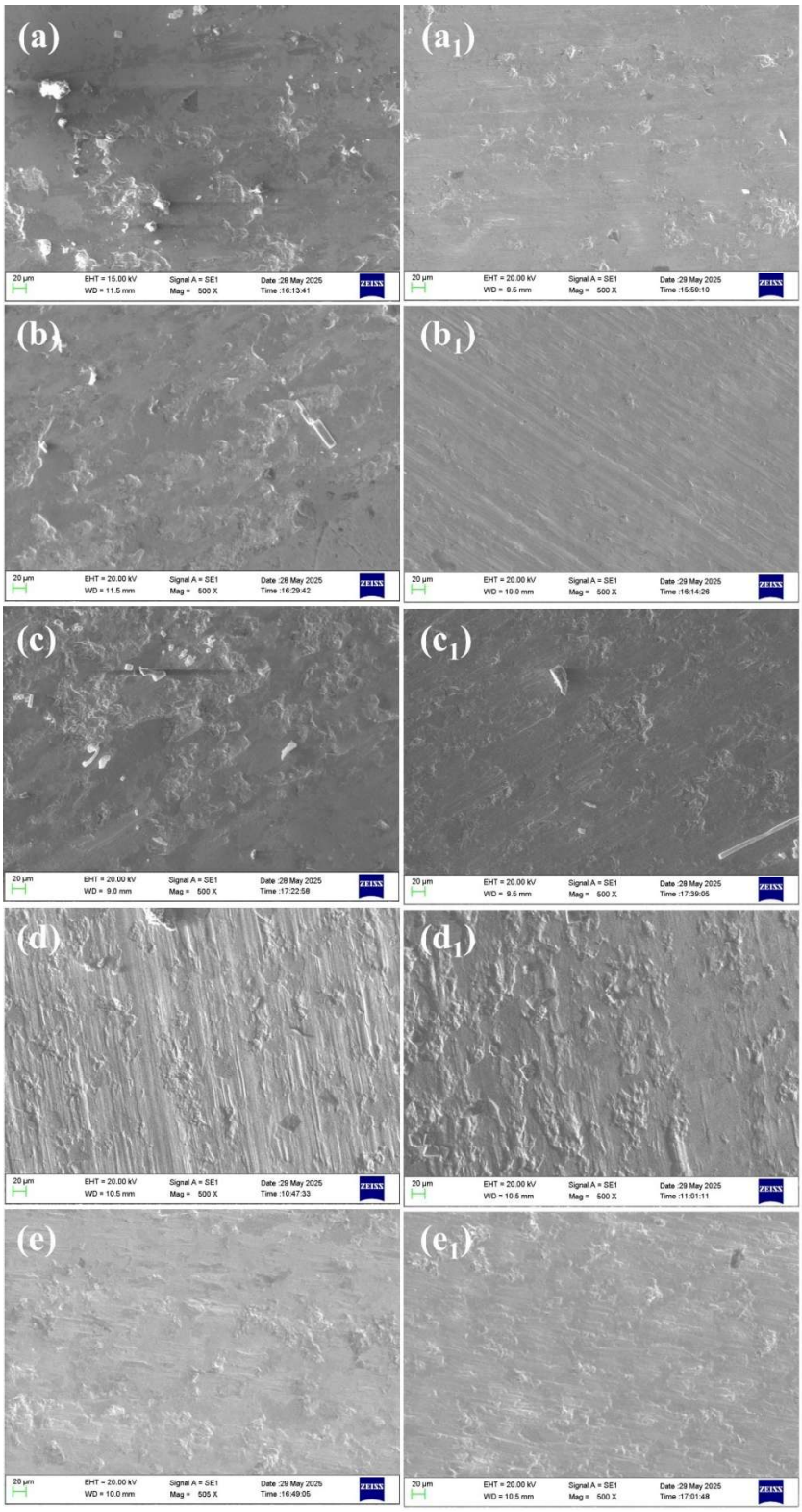


**Fig. 6.12:** Worn surfaces of (a) Ti-5Nb, (b) Ti-10Nb, (c) Ti-15Nb, (d) Ti-20Nb, (e) Ti-25Nb after OCP, and corresponding ($a_1$-$e_1$) for PDP tribocorrosion test

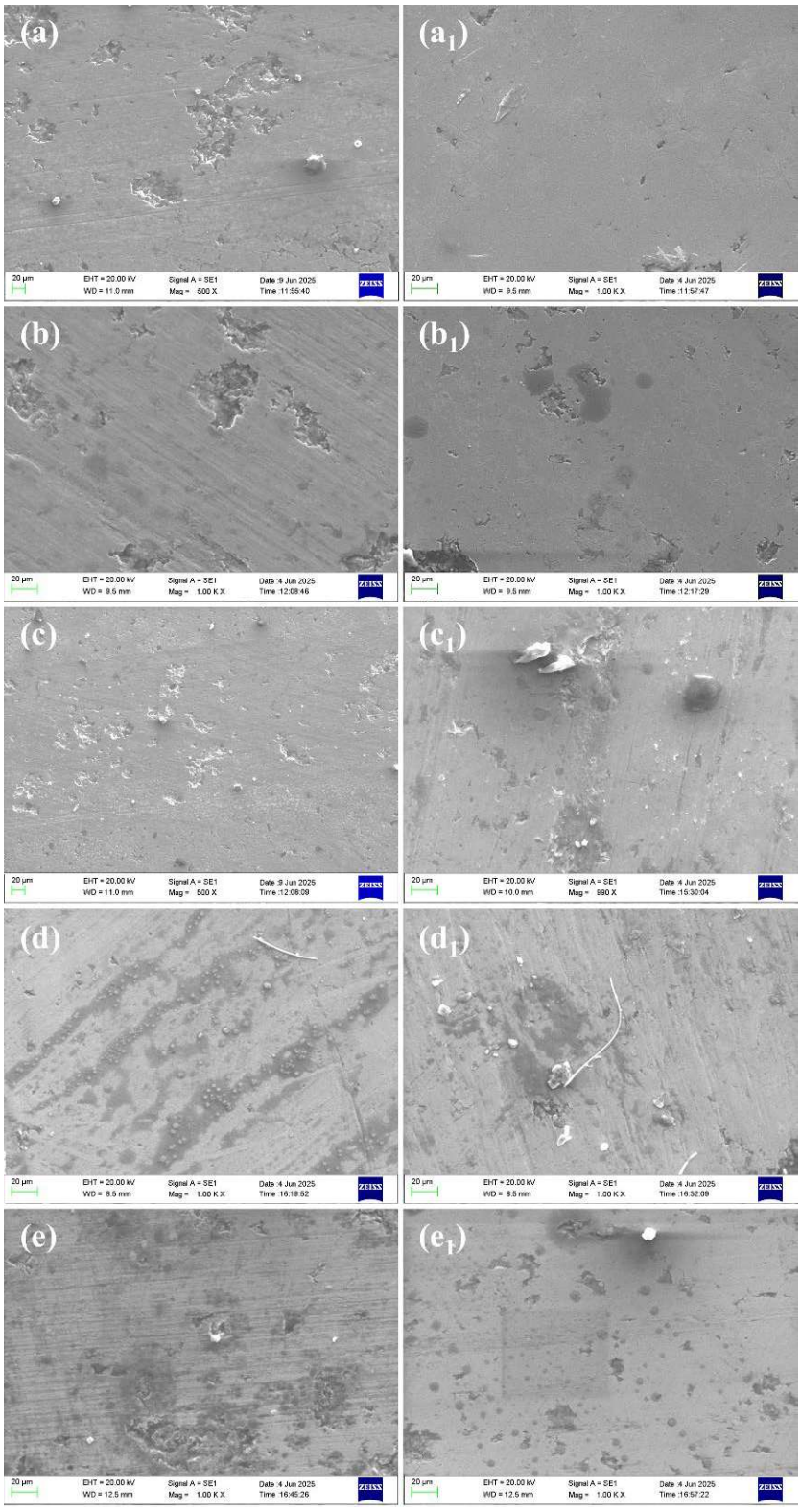


**Fig. 6.13:** Worn surfaces of (a) Ti-5Zr, (b) Ti-10Zr, (c) Ti-15Zr, (d) Ti-20Zr, (e) Ti-25Zr after OCP, and corresponding ($a_1$-$e_1$) for PDP tribocorrosion test

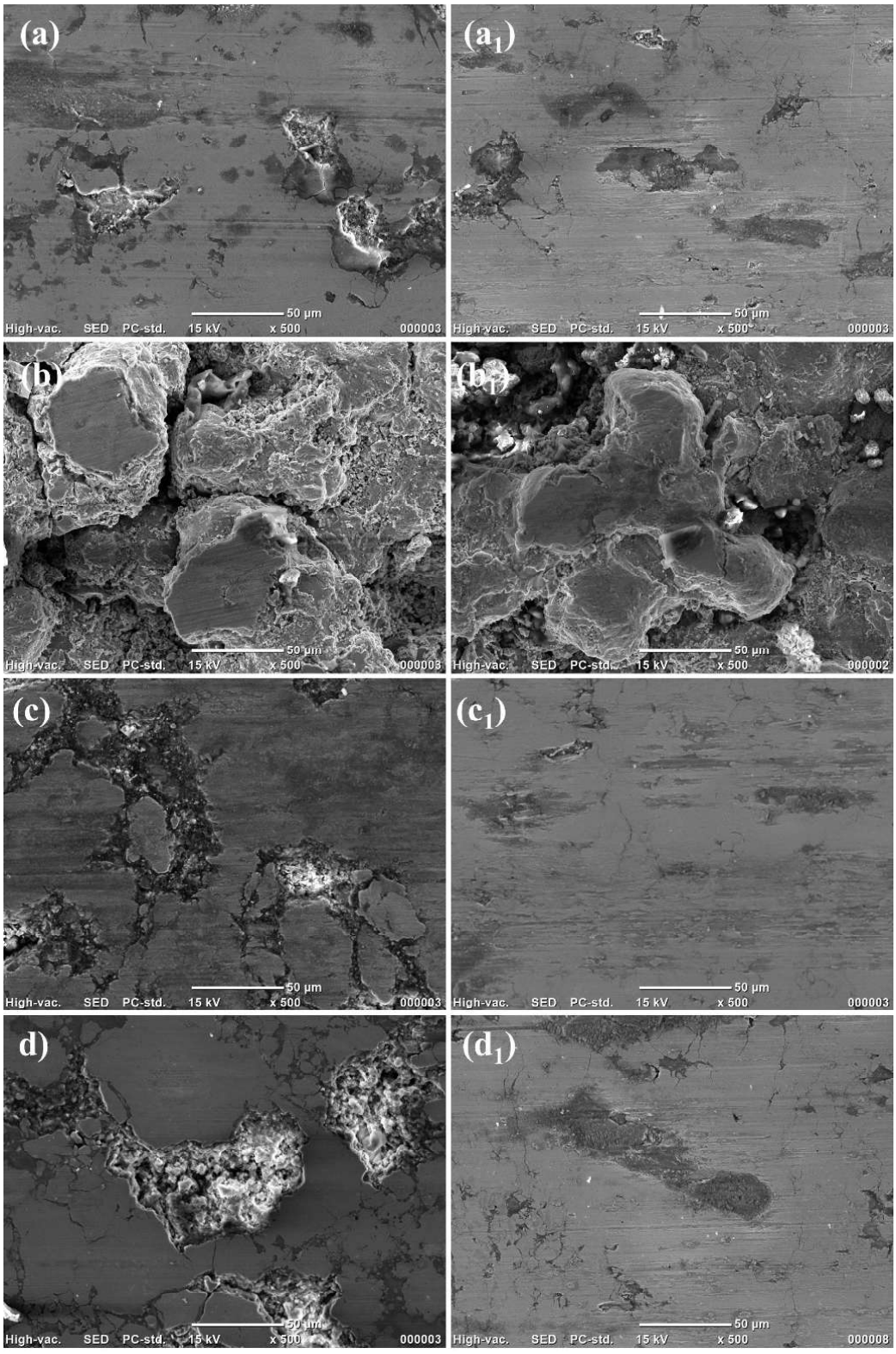


**Fig. 6.14:** Worn surfaces of (a) Ti-10Zr-5Nb, (b) Ti-10Zr-10Nb, (c) Ti-10Zr-15Nb, (d) Ti-10Zr-20Nb after OCP, and corresponding ($a_1$-$d_1$) for PDP tribocorrosion test

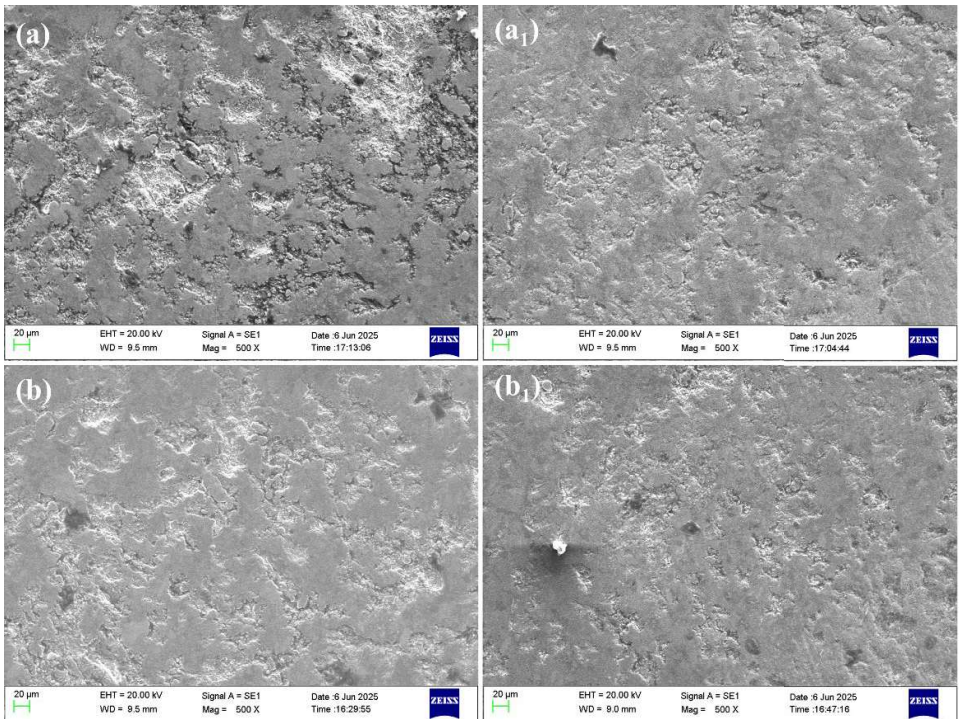


**Fig. 6.15:** Worn surfaces of (a) $TiNb_{1.5}Mo_{1.1}Zr_{1.15}Cu_{0.25}$, (b) $TiNbZr_{0.8}Mo_{0.92}Sn_{0.28}$after OCP, and corresponding ($a_1$-$b_1$) for PDP tribocorrosion test

### 6.6 Summary of chapter

This chapter presents a comprehensive evaluation of the tribocorrosion behavior of cpTi, Ti-6Al-4V, and various developed alloys under simulated physiological conditions using OCP and PDP tests. Among the reference materials, Ti-6Al-4V outperformed cpTi due to its superior passivation and reduced wear, attributed to the presence of Al and V. In the binary alloy series, Ti-10Nb demonstrated the best tribocorrosion resistance with the lowest wear volume and stable electrochemical response, making it a promising candidate for biomedical applications. For Ti-xZr alloys, Ti-15Zr exhibited optimal performance, showing the lowest wear scar width and volume under both OCP and PDP conditions. In the ternary system, Ti-10Zr-15Nb showed a favorable balance of wear and corrosion resistance, particularly under PDP conditions, where the wear volume significantly decreased, likely due to lubricating

debris and improved passivation. High-entropy alloys, particularly the Cu-containing variant, showed better tribocorrosion resistance under PDP conditions due to the formation of stable passive films. Overall, the ternary alloy Ti-10Zr-15Nb and binary alloy Ti-10Nb were found to be the most suitable for biomedical applications, offering a balanced synergy between mechanical wear resistance and electrochemical stability, which is crucial for long-term implant performance.